35th Annual International Conference of the IEEE EMBS
Osaka, Japan, 3 - 7 July, 2013

Retinal ganglion cells electrophysiology: the effect of cell morphology on impulse waveform

Matias I. Maturana[3,6], Raymond Wong[1,2], Shaun L. Cloherty[1,2,7], Michael R. Ibbotson[1,2,7], Alex E. Hadjinicolaou[1,2,*], David B. Grayden[3,4,5,6], Anthony N. Burkitt[3,4,5,6], Hamish Meffin[3,4,6], Brendan J. O'Brien[1,2,7], Tatiana Kameneva[3,4,6,*]

Abstract— **There are 16 morphologically defined classes of rats retinal ganglion cells (RGCs). Using computer simulation of a realistic anatomically correct A1 mouse RGC, we investigate the effect of the cell′s morphology on its impulse waveform, using the first-, and second-order time derivatives as well as the phase plot features. Using whole cell patch clamp recordings, we recorded the impulse waveform for each of the rat RGCs types. While we found some clear differences in many features of the impulse waveforms for A2 and B2 cells compared to other cell classes, many cell types did not show clear differences.**

I. INTRODUCTION

Retinal ganglion cells (RGCs) have been categorized into morphological classes in a number of species, including rats [11], cats [2], monkey [6] and rabbits [16]. The classification criteria commonly used are the soma and dendrites size, dendritic field diameter and angle of the dendritic stratifications. The similarities in the intrinsic electrophysiology between homologous morphological classes in different species (cats and rats) have been explored in [21]. The correspondence between morphological and electrophysiological classification has been explored in [15], [20]. How the morphological properties of mice RGCs relate to the stratification pattern of the dendrite is explored in [5]. There are 16 morphologically defined classes of rats RGCs [11]. The focus of this paper is upon the analysis of rat RGCs.

The action potential waveform in many neurons consists of several components, that can be determined by examining the first- and second-order derivatives of the membrane potential [3], [13], [14]. In this paper we focus on this technique as an objective method to analyze the impulse waveform for different morphological RGCs types. In addition, we analyze the features of the phase plot, which shows the rate of change of the membrane potential against the membrane potential itself. It has been shown that for recordings made at the soma, the first peak in the second-order derivative arises from the axonal spike arriving at the site of the recording; the time between the first and the second peak in the second-order derivative corresponds to the time it takes to fully activate somatic sodium channels (time to charge soma capacitance). The second peak in the second-order derivative corresponds to the maximal recruitment of somatic sodium channels [3], [13], [14].

Phase plot analysis allows to measure the subtle differences in the impulse waveform, such as the initial segment-soma/dendritic break (ISSD), that correspond to the early rising phase of the action potential. When the recording is made at the soma, the presence of the ISSD in the phase plot indicates that the impulse was initiated at a region neighboring to the soma that has a lower threshold [4]. The shallow phase plot usually suggests that the action potential initiation site is at the soma rather than at the axon initial segment. The site of action potential initiation is an active area of research [10], [12]. The ISSD break is a purely electrotonic effect at the soma due to the lower threshold of the axon initial segment [8].

How the sodium, potassium, and calcium voltage-gated channel density in different morphological compartments, electrotonic current and temperature affect the features of the phase plot is explored in [8], [17]. In this paper, we investigate the effect of a RGC′s morphology on its impulse waveform using computer simulation of RGCs that are anatomically correct. In addition, using experimental recordings from 90 rat RGCs, we investigated the effect of the morphology of different classes RGCs on some features of their impulse waveforms.

II. METHODS

A. Simulation

The multicompartment mouse RGC structure was obtained from the NeuroMorpho database [1]. It was shown that mice and rats cell types are similar [13]. The cell was classified as A1 based on the soma and dendritic diameter, soma shape, dendritic stratification and length. The membrane properties were described using Hodgkin-Huxley type equations:

$$C_{\mathrm{m}}\frac{dV}{dt} = I_{\mathrm{L}} + I_{\mathrm{Na}} + I_{\mathrm{Ca}} + I_{\mathrm{K}} + I_{\mathrm{K,A}} + I_{\mathrm{K(Ca)}} + I_{\mathrm{stim}}, \quad (1)$$

where V is the membrane potential, C_{m} is the specific capacitance of the membrane, and I_{stim} is intracellular stimulation current. Leak (I_{L}), sodium (I_{Na}), calcium (I_{Ca}), delayed rectifier (I_{K}), A-type ($I_{\mathrm{K,A}}$), and Ca-activated ($I_{\mathrm{K(Ca)}}$) potassium currents had dynamics as described by [9]. All parameters were taken as in [9]. The effect of the following parameters on the phase plot was investigated:

[1] The National Vision Research Institute, [2] Australian National University, [3] NeuroEngineering Laboratory, Department of Electrical Electronic Engineering, the University of Melbourne. [4] NICTA Victoria Research Lab. [5] Bionics Institute. [6] Center for Neural Engineering, the University of Melbourne. [7] Optometry and Vision Science, the University of Melbourne.*tkam@unimelb.edu.au

978-1-4577-0216-7/13/$26.00 ©2013 IEEE

- Sodium channel band (SOCB) location: SOCB distance from the soma was varied from 15 to 80 μm in 15 μm steps.
- Base potassium conductance ($\bar{g}_{\mathrm{K}}$): $\bar{g}_{\mathrm{K}}$ in the soma was increased from the soma from 0.03 to 0.1 S/cm^2 in 0.007 S/cm^2 steps. Potassium conductance in all other compartments varied in the proportion of the soma conductance as discussed in [9].
- Potassium conductance in the dendrites. According to [9], $\bar{g}_{\mathrm{K}}^{\mathrm{dendrites}} = 0.5K\bar{g}_{\mathrm{K}}^{\mathrm{soma}}$, where $K = 1$. In this study, K was varied from 0.15 to 1.5 S/cm^2 in 0.15 S/cm^2 steps.
- Sodium ($\bar{g}_{\mathrm{Na}}$) conductance in the dendrites. According to [9], $\bar{g}_{\mathrm{Na}}^{\mathrm{dendrites}} = 0.5N\bar{g}_{\mathrm{Na}}^{\mathrm{soma}}$, where $N = 1$. In this study, N was varied from 0.15 to 1.5 in 0.15 S/cm^2 steps.

The first- and second-order time derivatives of the membrane potential were calculated at each time point. The derivatives were calculated using the central difference algorithm. The ISSD break was defined as the point in the first-order derivative where the second-order derivative reaches a minimum: ie. the point in the phase plot where the gradient is a minimum. The trough refers to the trough in the second-order derivative between the two peaks (the lowest part of the second-order derivative wave). Refer to Fig. 1 for graphical interpretation. Cells responses were simulated in the NEURON environment (Hines 1993). Data was analyzed in Matlab.

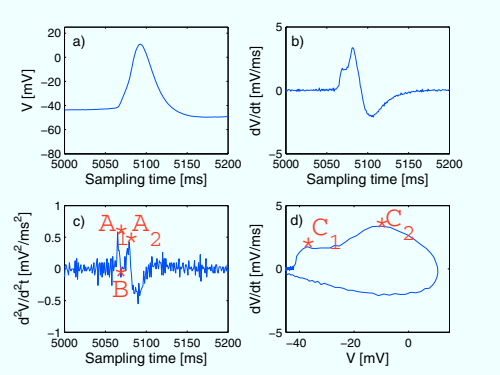

Fig. 1. Graphical interpretation of the data used for analysis. a) Experimentally recorded membrane potential of an A2i (inner) cell, b) First-order time-derivative of the membrane potential, c) Second-order time-derivative of the membrane potential, d) Phase plot. A_1, A_2 and B two peaks and a trough in the second-order derivative used for analysis. C_1, C_2 two peaks in the phase plot used for analysis.

B. Experiments

Whole-cell current clamp recordings from 90 RGCs were obtained using procedures described previously [15], [20]. Data was obtained from Long Evans rats aged between 3 and 15 month. Recordings were made at room temperature. Physiological data were acquired at 20kHz using custom software developed in LabView (National Instruments). Cells were excluded from analysis if they exhibited markedly inconsistent responses to stimuli, or if their morphological classification could not be reliably ascertained after performing the immunocytochemistry. Filled RGCs were reconstructed in 3D with a confocal microscope (Zeiss PASCAL) and classified morphologically into morphological types according to the criteria described in [11], [18]. The number of cells used for analysis and number of recordings for each morphological class is shown in Fig. 2. RGCs responses

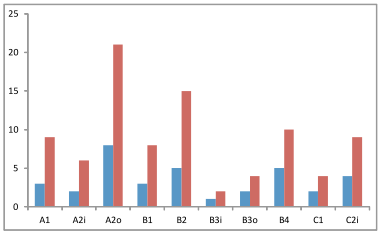

Fig. 2. Number of cells used for analysis (blue) and number of recordings (red) for each morphological class.

were tested with a series of depolarizing current steps of 400 ms duration. Spontaneous spikes or spikes evoked by just-threshold current were used for analysis. If a spike was elicited leass than approximately 100 ms after the current injection time, the data for such recording was discarded. This protocol was used because in this case it was difficult to judge if a spike was elicited by the threshold current (therefore may be similar in shape to a spontaneous spike) or this was a spike elicited by a current injection and therefore had distinct properties from the spontaneous spike. For each of the recordings the following was analyzed:

- The amplitude and time of the trough between the peaks in the second-order derivative.
- The difference between the first peak and the trough in the second-order derivative.

III. Results

A. Simulation

Sodium channel band (SOCB) location. Fig. 3.a shows that as the SOCB moves away from the soma, the ISSD break becomes more pronounced, resulting in a larger ISSD break with a deeper trough between the two peaks in the phase plot. Fig. 3.b shows an emergence of an initial peak with a deeper trough between the two peaks in the second-order derivative as the distance of the SOCB from the soma is increased. Similar result was shown experimentally in [13]. This occurs because there is a larger number of sodium channels between the soma and low threshold region as the SOCB is moved away from the soma. This results in a larger initial current invading the soma at the onset of the action potential.

Base potassium conductance. Fig. 4.a shows a deeper trough between the two peaks, a lowering of the maximal peak, and a higher peak in the re-polarizing phase in the phase plot with increasing conductance of potassium in the soma. Fig. 4.b shows a deeper trough between the two peaks in the second-order derivative when the potassium conductance in the soma is increased. This occurs because there is a larger number of potassium channels being activated during the onset of the action potential (as the action

potential reaches approximately -30 mV) that inhibits the depolarization of the cell, resulting in a lower trough in the two plots and a lower maximal peak in the phase plot. A larger number of potassium channels also results in a faster return to the resting potential in the re-polarizing phase of the plot. As a result, the spike width (spike width at half height) becomes shorter.

Dendritic potassium conductance. Fig. 5.a shows a reduction in the maximal peak and the emergence of a trough between the ISSD break and the maximal peak in the phase plot with increasing concentration of potassium in the dendrites. Fig. 5.b shows a large reduction in the maximal peak and the emergence of the initial (small) peak.

Dendritic sodium conductance. Fig. 6.a shows an increase in the maximum peak of the phase plot when the conductance of sodium in the dendrites is increased. The second-order derivative shows a large increase in the maximal peak and the disappearance of the initial peak when the conductance of sodium in the dendrites is increased. The maximal peak becomes much larger, and the first peak disappears entirely, refer to Fig. 6.b.

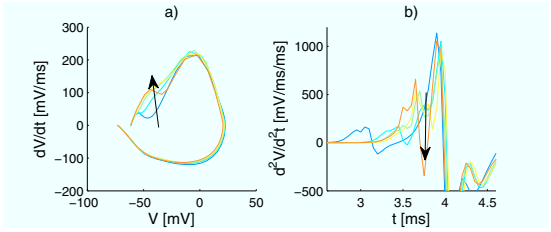

Fig. 3. The effect of the SOCB location on a) the phase plot, and b) the second-order derivative. Traces change from blue to red as the SOCB distance from the soma changes from 15 to 80 μm in 15 μm steps.

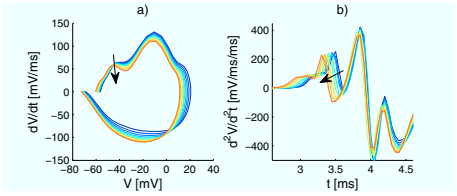

Fig. 4. The effect of the base potassium conductance value in the soma on a) the phase plot, and b) the second-order derivative. Potassium conductance in all other compartments varied in the proportion of the soma conductance as discussed in [9]. Traces change from blue to red as $\bar{g}_{\mathrm{K}}$ in the soma is increased from 0.03 to 0.1 S/cm^2 in 0.007 S/cm^2 steps.

B. Experiments

We found that some morphological classes have some features in their impulse waveforms that are distinct from other classes. A comparison of the phase plots for two cells that have ISSD break and those that do not is given in Fig. 7. Due to space constraints, we present data on the amplitude of the trough in the second-order derivative only. Fig. 8 shows the amplitude of the trough in the second-order derivative for different classes of RGCs. This histogram is informative of the ISSD break. If the trough in the second derivative reaches zero or is below zero, then the ISSD break becomes

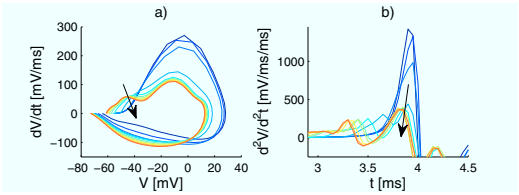

Fig. 5. The effect of the potassium conductance value in the dendrites on a) the phase plot, and b) the second-order derivative (b). Traces change from blue to red as the $\bar{g}_{\mathrm{K}}$ in the soma is increased.

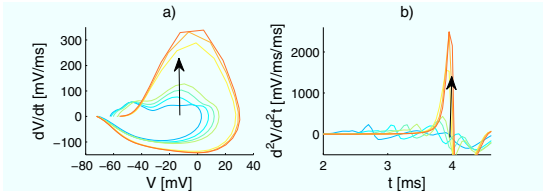

Fig. 6. The effect of the sodium conductance value in the dendrites on a) the phase plot, and b) the second-order derivative (b). Traces change from blue to red as the $\bar{g}_{\mathrm{Na}}$ in the soma is increased.

visually well defined (that is if the first peak is also present). If the trough is above zero, then it becomes harder to see the ISSD break. Note a large positive amplitude of the trough for A2 cells. The difference between the first peak and the trough in the second-order derivative is given in Fig. 9 that shows that B2 cells have a clear distinction from all other cells except A2i.

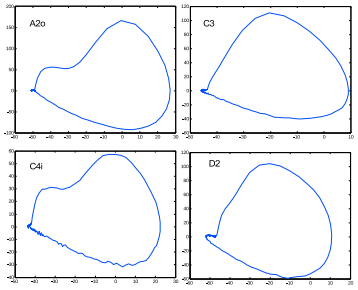

Fig. 7. Phase plot for two cells with the ISSD break (a2o, c4i) and those without (c3, d2). Horizontal axis: membrane potential [mV], vertical axis: first-order derivative of the membrane potential [mV/ms]

IV. Discussion and Conclusion

Using computer simulation of a multicompartment morphologically correct A1 mouse cell, we investigated the effects of the cell′s biophysical properties on its impulse waveform. we found that the ISSD break becomes more pronounced as the SOCB moves away from the soma. This result may lead to the prediction of the location of the SOCB based on the recordings of the impulse waveform. We analyzed experimentally recorded membrane potential data for different morphological classes of RGCs. While we found some clear differences in many features of the impulse waveforms for A2 and B2 cells compared to other cell classes, many cell types did not show clear differences

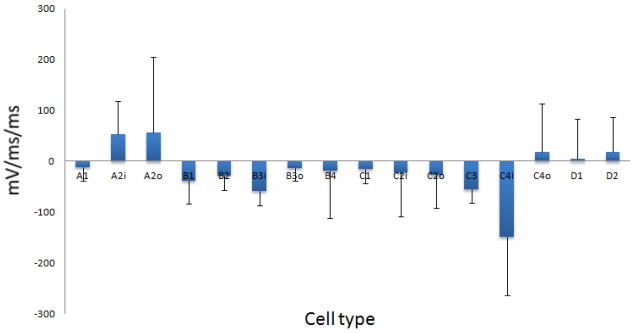

Fig. 8. The histogram of the amplitude of the trough in the second-order derivative for different classes of RGCs.

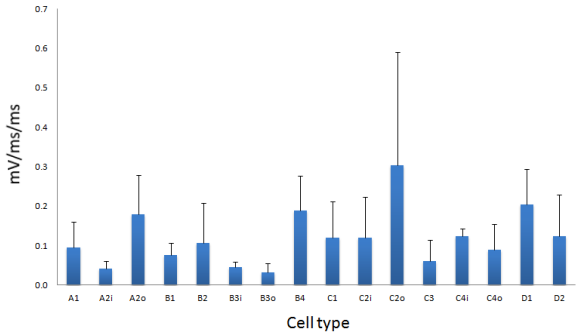

Fig. 9. The histogram of the normalized difference between the first peak and the trough in the second-order derivative.

and the error bars were large. This may be due to a sample size.

In simulation, we found that potassium channel concentration changes in the soma and in the dendrites have different effects. While changing potassium conductance in the soma has only small effects on the phase plot, changing dendritic potassium concentration has dramatic changes in the maximum peak, trough and shape of the phase plot. The higher the dendritic potassium concentration is, the longer the cell takes to respond (refer to the time difference between peaks in second derivative, and the amplitude of the second peak in the second derivative in Fig. 5). Similar to potassium concentration changes in dendrites, the sodium conductance changes in the dendrites have a large effect on the maximum peak in phase plot. This may imply that dendritic electrophysiology may have a large effect on the impulse waveform.

In simulation, we found that the ISSD break becomes more pronounced in the phase plot with the increased distance of the SOCB from the soma. This result was shown experimentally in [13]. This is due to the fact that if the initial segment is far enough from the soma results in the local channels being not involved before the spike invades the soma. Based on the timing and amplitude of two peaks in the second-order derivative of the membrane potential, it may be possible to cluster cells based on the features of the ISSD break. Since the features of the ISSD break correspond to the site of the action potential initiation, this may lead to the classification of the cells based on the impulse initiation site. This may have important implications for a visual prosthesis, such as finding a stimulation strategy to activate cell types selectively.

V. Acknowledgments

The authors wish to thank Emily O'Brien for her help classifying A1 mice RGC cell for simulations. This research was supported by the Australian Research Council (ARC) through its Special Research Initiative (SRI) in Bionic Vision Science and Technology grant to Bionic Vision Australia (BVA). The Bionics Institute acknowledges the support it receives from the Victorian Government through its Operational Infrastructure Support Program. This research was supported by NHMRC Project grant 585440 and ARC Discovery grant DP0881247.

References

[1] G.A. Ascoli, D.E. Donohue, M. Halavi. NeuroMorpho.Org: a central resource for neuronal morphologies. J. Neurosci., 27(35): 9247-9251, 2007.

[2] B.B. Boycott, H. Wassle. The morphological types of ganglion cells of the domestic cat′s retina. *J. Physiol.,* 240: 397 -419, 1974.

[3] C.M. Colbert, D. Johnston. Axonal action-potential initiation and Na^+ channel densities in the soma and axon initial segment of subicular pyramidal neurons. *J. Neurosci.,* 16: 6676 - 6686, 1996.

[4] J.S. Coombs, D.R. Curtis, J.C. Eccles. Theinterpretation of spike potential of motoneurons. *J. Neurophysiol.,* 139: 198 - 231, 1957.

[5] Coombs J, van der List D, Wang GY, Chalupa LM. Morphological properties of mouse retinal ganglion cells. *J. Neurosci.,* 140(1): 123-136, 2006.

[6] D.M. Dacey, B.B. Peterson, F.R. Robinson, P.D. Gamlin. Fireworks in the primate retina: in vitro photodynamics reveals diverse LGN-projecting ganglion cell types. *Neuron*, 37: 15 - 27, 2003.

[7] R. Fitzhugh. Mathematical model for excitation and propagation in nerve. Biological Engineering. *New York: McGray Hill,* 1969.

[8] J.F. Fohlmeister, E.D. Cohen, E.A. Newman. Mechanisms and distribution of ion channels in retinal ganglion cells: using temperature as an independent variable. *J. Neurophysiol.,* 103: 1357 - 1374, 2010.

[9] J.F. Fohlmeister, R.F. Miller. Mechanisms by which cell geometry controls repetitive impulse firing in retinal ganglion cells. *J. Neurophysiol.,* 78(4): 1948-1964, 1997.

[10] S. I. Fried, A. C. W. Lasker, N. J. Desai, D. K. Eddington, J. F. Rizzo 3rd. Axonal sodium-channel bands shape the response to electric stimulation in retinal ganglion cells. *J. Neurophys.,* 101: 1972 - 1987, 2009.

[11] K.R. Huxlin, A.K. Goodchild. Retinal ganglion cells in the albino rat: Revised morphological classification. *J. Comparat. Neurol.,* 385: 309 - 323, 1997.

[12] M.H. Kole, S.U. Ilschner, B.M. Kampa, S.R. Williams, P.C. Ruben, G.J. Stuart. Action potential generation requires a high sodium channel density in the axon initial segment. *Nat. Neurosci.,* 11: 178 - 186, 2008.

[13] G. J. Kress, M.J. Dowling, J.P. Meeks, S. Mennerick. High threshold, proximal initiation, and slow conduction velocity of action potentials in dentate granule neuron mossy fibers. *J. Neurophys.,* 100: 281 - 291, 2008.

[14] J.P. Meeks, S. Mennerick. Action potential initiation and propagation in CA3 pyramidal axons. *J. Neurophysiol.,* 97: 3460 - 3472, 2007.

[15] B.J. O'Brien, T.Isayama, R. Richardson, D.M. Berson. Intrinsic physiological properties of cat retinal ganglion cells. *J. Physiol.*, 538.3: 787-802, 2002.

[16] R.L. Rocklin, F.J. Daly, M.A. MacNeil, S.P. Brown R.H. MAsland. The diversity of ganglion cells in a mammalian retina. *J. Neurophys.,* 22: 3831 - 3843, 2002.

[17] B.W. Sheasby, J.F. Fohlmeister. Impulse encoding across the dendritic morphologies of retinal ganglion cells. *J. Neurophysiol.,* 81: 1685-1698, 1999.

[18] W.Z. Sun, N. Li, S.G. He. Large-scale morphological survey of mouse retinal ganglion cells. *Vis. Neurosci.,* 19: 483 - 493, 2002.

[19] H. Wassle Parallel processing in mammalian retina. *Nature Reviews Neurosci,* 5: 1 - 11, 2004.

[20] R.C. Wong, S.L. Cloherty, M.R. Ibbotson, B.J. O'Brien. Intrinsic physiological properties of rat retinal ganglion cells with a comparative analysis. *J. Neurophys.*, 108: 2008 - 2023, 2012.

[21] R.C. Wong, S.L. Cloherty, M.R. Ibbotson, B.J. O'Brien. Are retinal ganglion cell intrinsic phyciological properties conserved? *e-abstract, ARVO 2011.*